JOURNAL OF GEOPHYSICAL RESEARCH, VOL. 115, A04106, doi:10.1029/2009JA014680, 2010

Langmuir waves upstream of interplanetary shocks: Dependence on shock and plasma parameters

M. P. Pulupa,[1] S. D. Bale,[1] and J. C. Kasper[2]

Received 24 July 2009; revised 29 October 2009; accepted 3 December 2009; published 29 April 2010.

[1] We have examined 178 interplanetary shocks observed by the Wind spacecraft to establish which shock and plasma parameters are favorable for the production of upstream Langmuir waves and therefore to determine which shocks are likely to generate interplanetary Type II radio bursts. Of the 178 shocks included in this study, 43 produced upstream Langmuir waves, as evinced by enhancements in wave power near the plasma frequency. The large number of observed shocks permits the use of statistical tests to determine which parameters control the upstream activity. The best predictor of activity is the de Hoffmann-Teller speed, a result consistent with the fast Fermi model of electron acceleration. Several other parameters, including the magnetic field strength and the level of solar activity (but not the Mach number), are also correlated with upstream activity. These additional parameters may be associated with an increased level of shock front curvature or upstream structure, leading to the formation of upstream foreshock regions, or with the generation of an upstream electron population favorable for shock reflection.

Citation: Pulupa, M. P., S. D. Bale, and J. C. Kasper (2010), Langmuir waves upstream of interplanetary shocks: Dependence on shock and plasma parameters, *J. Geophys. Res.*, *115*, A04106, doi:10.1029/2009JA014680.

1. Introduction

[2] Interplanetary (IP) shocks, which are often driven by IP coronal mass ejections (ICMEs), accelerate solar wind electrons into foreshock regions upstream of the shock. These regions are in some respects analogous to the foreshock regions upstream of the bow shocks of magnetized bodies in the solar wind. In both types of foreshock region, the reflected electron beams create unstable bump-on-tail electron distribution functions, which excite a Landau resonance and create electrostatic oscillations known as Langmuir waves. The Langmuir waves undergo a mode conversion process and generate electromagnetic radio waves at the plasma frequency f_p and $2f_p$. These radio waves propagate throughout the heliosphere and are used as a remote diagnostic of electron acceleration at shocks. As an IP shock propagates radially outward from the sun, the plasma becomes less dense and the plasma frequency decreases. The radio emission generated upstream of the shock is observed on a radio spectrogram as a slowly drifting, often patchy feature known as an IP Type II radio burst.

[3] IP Type II radio bursts are a primary method used to track the progress of CME-driven shocks through the heliosphere. The decrease in the frequency of Type II emission due to the decrease in local electron density, together with an assumed radial electron density profile, can be used to measure the velocity of the shock [*Cane et al.*, 1982], and this measurement can be used as a tool in space weather forecasting [*Cremades et al.*, 2007]. In addition to measurements of radial speed, direction finding techniques can be used to provide information about the three-dimensional structure of the shock [*Hoang et al.*, 1998; *Reiner et al.*, 1998].

[4] It is still a matter of debate where on the CME-driven shock surface the Type II burst is being generated. It would be very valuable to know if Type II emission is generated where the shock compression is strongest, or where the shock front and upstream magnetic field are favorably aligned, as that would allow us to determine if the emission is always at the nose of the shock, or if it can also occur on the flanks or on the trailing edges. This work is complementary to the direction finding technique of probing Type II burst origins, in that it focuses on direct measurements of the process in situ instead of remote reconstruction.

[5] Investigation of IP foreshock regions is guided by previous studies of the terrestrial electron foreshock region. The terrestrial electron foreshock is a commonly observed feature of the quasiperpendicular terrestrial bow shock, and copious in situ measurements of electron beams and electrostatic oscillations present in the terrestrial foreshock have been made for several decades. Upstream electrons originating at the bow shock accompanied by plasma frequency noise were observed by the IMP and OGO spacecraft [*Anderson*, 1968; *Scarf et al.*, 1971]. Further upstream observations of electron beams [*Anderson et al.*, 1979; *Feldman et al.*, 1983] and in situ measurements of Langmuir waves [*Filbert and Kellogg*, 1979] were made by the ISEE and IMP spacecraft. These early measurements confirmed

[1]Department of Physics and Space Sciences Laboratory, University of California, Berkeley, California, USA.
[2]Harvard-Smithsonian Center for Astrophysics, Cambridge, Massachusetts, USA.

0148-0227/10/2009JA014680

that the electron beams appear upstream of the shock when the spacecraft is magnetically connected to the quasi-perpendicular bow shock. These observations also established the spatial structure of the electron foreshock, showing that the strongest electron beams and the most intense Langmuir waves occur near the edge of the electron foreshock, where the upstream magnetic field is very nearly perpendicular to the shock normal.

[6] Langmuir waves [*Gurnett et al.*, 1979] and reflected electrons [*Potter*, 1981] were observed upstream of IP shocks, lending the support of in situ evidence to the theory of the generation of IP Type II bursts by shock accelerated electrons [*Cane et al.*, 1981, 1987]. However, unambiguous in situ observation of Type II source regions, including both wave observations and plasma data which resolve the accelerated electron beams, as first reported by *Bale et al.* [1999], is rare. This comparative rarity is mainly due to the necessity of high time resolution plasma measurements to resolve the velocity dispersed electron beams which are characteristic of upstream foreshock regions. A previous study [*Pulupa and Bale*, 2008] made use of high cadence "burst mode" electron measurements to resolve the velocity dispersion of the electron beams and thereby measure the dimensions of the foreshock region. However, burst mode data is unavailable for the majority of shocks observed by the Wind spacecraft, and of the shocks with burst mode data, only three presented time-resolved velocity dispersed beams.

[7] *Wilson et al.* [2007] used the Time Domain Sampler (TDS) instrument from the Wind/WAVES plasma wave experiment [*Bougeret et al.*, 1995] to study the occurrence of electrostatic waves in the vicinity of interplanetary shocks, showing that the strongest waves occur in the shock ramp itself, and in particular that the shock ramp is dominated by large amplitude ion acoustic waves. TDS selects specific waveform events to send in the telemetry stream, and the selection algorithm preferentially selects large amplitude events. Due to this selection effect, two shocks with similar levels of upstream Langmuir wave activity (LWA) could appear different in the TDS data stream, depending on the level of ion acoustic waves in the ramp or downstream region. Therefore, in order to search for upstream Langmuir waves, we use the low-frequency (4–256 kHz) Thermal Noise Receiver (TNR) from Wind/WAVES, which offers continuous coverage in the upstream region and a uniform measurement of upstream activity at each shock. Langmuir waves are apparent in a TNR spectrogram as intense enhancements of wave power at the plasma frequency, and the presence of upstream Langmuir waves is a signature of IP foreshock regions [*Bale et al.*, 1999; *Fitzenreiter et al.*, 2003].

[8] A similar method was employed by *Thejappa and MacDowall* [2000], who used data from the Ulysses Unified Radio and Plasma experiment to search for Langmuir waves in the vicinity of IP shocks. *Thejappa and MacDowall* [2000] found that Langmuir waves exist (1) primarily in the upstream region, (2) at both quasiperpendicular and quasi-parallel shocks, and (3) primarily at supercritical shocks.

[9] For any given shock crossing by a single spacecraft, the presence or absence of upstream LWA is largely determined by the local shock geometry. Furthermore, the measurements of local shock parameters made at the crossing point will be different from those at the quasi-perpendicular acceleration point of the electron beam, introducing uncertainty into the calculation of these parameters and their effect on the acceleration process. Therefore, in order to investigate the effects of different local and global shock parameters, as well as the locally measured solar wind parameters, it is necessary to examine many shocks. Wind has been in continuous operation since 1994, and has observed a sufficient number of IP shock crossings to determine statistically which parameters control the production of upstream Langmuir waves.

[10] The structure of the remainder of this paper is as follows: Section 2 presents a brief review of the fast Fermi theory of electron reflection at heliospheric shocks. Section 3 discusses the database of Wind IP shocks examined in this study, and explains the algorithm used to automatically determine which shocks exhibit Langmuir waves in the upstream region. Section 4 describes the shock and plasma parameters computed for each shock, and how the parameters relate to electron acceleration and the generation of foreshock regions. Section 5 describes the results, showing which of the calculated parameters control the generation of upstream Langmuir waves, and section 6 briefly discusses the implications of these results for the broader theory of Type II radio bursts.

2. Brief Review of Fast Fermi Theory

[11] The fast Fermi (called "fast" because the energization takes place in a single encounter, rather than the multiple encounters of classic Fermi theory) model for the energization of thermal electrons at the terrestrial bow shock was derived independently by *Leroy and Mangeney* [1984] and *Wu* [1984]. The dynamics of electron acceleration in the fast Fermi model are most tractable in the de Hoffmann-Teller frame (HTF), in which the upstream plasma bulk velocity and magnetic field are parallel and therefore there is no upstream convective ($\mathbf{V} \times \mathbf{B}$) electric field. The energization of electrons in the upstream solar wind frame is a consequence of the boost to the HTF, the reflection, and the boost associated with the return to the solar wind frame.

[12] The transformation velocity to the HTF from the normal incidence frame (NIF), in which the upstream bulk velocity is antiparallel to the shock normal, is known as the de Hoffmann-Teller velocity, and is given by:

$$\mathbf{V}_{\mathrm{HT}} = \frac{\hat{\mathbf{n}} \times (\mathbf{V}_{\mathrm{u}} \times \mathbf{B}_{\mathrm{u}})}{\mathbf{B}_{\mathrm{u}} \cdot \hat{\mathbf{n}}} \tag{1}$$

[13] We denote quantities in the HT frame with a prime, e.g., the parallel $v'_{\parallel}$ and perpendicular $v'_{\perp}$ velocities. $\mathbf{V}_{\mathrm{HT}}$ lies in the shock plane parallel to the projection of the upstream magnetic field into the shock plane. An electron with incoming parallel velocity $v'_{\parallel}$ will be reflected upstream with a parallel velocity $-v'_{\parallel} + 2V_{\mathrm{HT}}$, and with an unchanged perpendicular velocity.

[14] The distribution of the reflected electrons is a loss cone distribution. The opening angle α of the cone is set by the ratio of upstream to downstream magnetic field, according to the relation $\alpha = \sin^{-1}(B_{\mathrm{u}}/B_{\mathrm{d}})$. The loss cone is modified by the presence of a frame-dependent potential

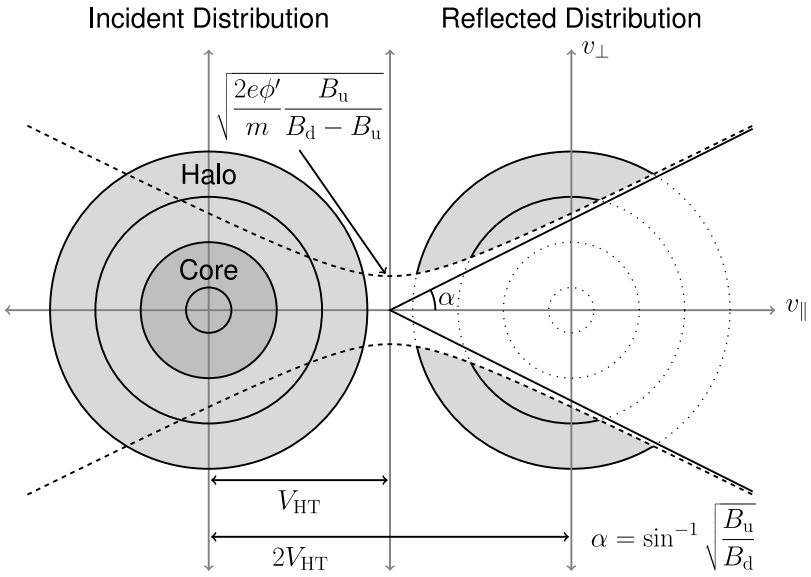

Figure 1. Diagram illustrating process for reflection of upstream electrons according to the theory of *Leroy and Mangeney* [1984] and *Wu* [1984]. The incident distribution is shown on the left in the solar wind frame. Electrons which lie above the separatrix determined by the cross shock potential and mirror ratio (described in equation (2)) are reflected, while the remaining electrons pass through the shock to the downstream region. The ratio V_{HT}/V_{th} is exaggerated compared to the measured ratio at a typical IP shock for clarity.

across the shock, resulting from the differential motion of protons and electrons through the shock layer. *Goodrich and Scudder* [1984] showed that electron energy gain is given by Φ', the cross shock potential in the HTF. Φ' affects the reflected distribution by drawing low energy electrons through the shock to the downstream region, broadening the loss cone for low values of $v'_\parallel$. This loss cone broadening has been observed in the terrestrial electron foreshock [*Larson et al.*, 1996].

[15] Assuming conservation of μ for the upstream electrons, the criterion for reflection in the HTF is:

$$\frac{1}{2}m\frac{v_\perp'^2}{B_u} \geq \frac{1}{B_d - B_u}\left(e\Phi' + \frac{1}{2}mv_\parallel'^2\right) \quad (2)$$

[16] The reflection criterion defines a separatrix in velocity space, which is plotted in Figure 1 as a dashed line. Electrons lying above the dashed line will be reflected, while those lying below will pass through the shock to the downstream region.

[17] The main difference between the two original papers describing the fast Fermi model is that *Leroy and Mangeney* [1984] included the effect of Φ' and used a single Maxwellian to model the electron population, while *Wu* [1984] did not include Φ' but included the effect of both the halo and core electron populations, using a bi-Maxwellian distribution. Despite these differences, the models yield similar results, and both concur that energization is most efficient when the angle θ_{bn} between the upstream magnetic field and the shock normal is almost 90°. Test particles injected into hybrid simulations of quasiperpendicular shocks have confirmed this dependence on θ_{bn} [*Krauss-Varban et al.*, 1989].

[18] Simulations of fast Fermi acceleration at nonplanar shocks, using parameters similar to those encountered at the terrestrial foreshock, show that parameters such as θ_{bn} can vary significantly during a reflection due to shock curvature. This variation limits the maximum energy of reflected electrons, but effects of this limitation on observed fluxes at a given energy are somewhat offset by focusing effects [*Krauss-Varban and Burgess*, 1991]. Curvature may also be important for IP foreshock regions, since the characteristic dimensions of these regions are on the order of the dimensions of the terrestrial bow shock [*Pulupa and Bale*, 2008].

[19] A model [*Knock et al.*, 2001] using the fast Fermi reflection mechanism to generate an electron beam and stochastic growth theory [*Cairns et al.*, 2000, and references within] to model the conversion of electron beam energy into radio emission has been applied to the foreshock region studied by *Bale et al.* [1999], and yields results consistent with observations. A refined version of this model [*Knock et al.*, 2003] predicts that foreshock emission is more likely to appear upstream of fast shocks, shocks with more upstream nonthermal electrons, shocks with large radii of curvature, and shocks which propagate through high-density upstream regions. Using Wind observations of a large number of shocks, we can compare these results with in situ data.

3. Shock Database and Langmuir Wave Detection Algorithm

[20] We use a database of IP shocks observed by Wind, containing 382 interplanetary shocks observed between 1996 and 2004. This IP shock database consists of determinations of the shock orientation and velocity, asymptotic upstream and downstream parameters, and more than fifty derived quantities including wave speeds and Mach

numbers. The database is available online (http://www.cfa.harvard.edu/shocks/) for multiple spacecraft, including Wind, and has been successfully used in previous studies of IP shocks ranging from solar cycle effects [*Richardson et al.*, 2006; *Zhang et al.*, 2007] to shock microphysics [*Wilson et al.*, 2007].

[21] We now briefly review the shock analysis methods employed in the database. We start with a merged data set of solar wind plasma and field observations from the Faraday Cup instruments and the Magnetic Field Investigation (MFI) Wind [*Ogilvie et al.*, 1995; *Lepping et al.*, 1995]. This database includes ion bulk properties including hydrogen and helium bulk velocities, densities, temperatures, and temperature anisotropies along with high-resolution magnetic field measurements averaged to coincide with the Faraday Cup observations. The data set is available publicly from the National Space Science Data Center and has been described in detail previously [*Kasper et al.*, 2006]. The solar wind observations are manually scanned for IP shocks, and candidate events exhibiting sudden changes in velocity, density, temperature, and magnetic field strength are added to the database. For each candidate event we then try to identify 10–15 minute long intervals of measurements upstream and downstream of the shock itself that are representative of asymptotic steady state conditions. Under the assumption that the IP shock is described by the fluid MHD equations and indeed is in a steady state, the change in the plasma parameters across the shock must satisfy the Rankine-Hugoniot (RH) jump conditions. We then follow the algorithms developed by *Vinas and Scudder* [1986] and *Szabo* [1994] and identify the shock orientation that best simultaneously satisfies all of the conserved quantities across the shock. In addition to the full RH method, we also employ the velocity and magnetic coplanarity techniques, and three mixed methods that use combinations of the changes of the magnetic field and velocity across the shock [*Abraham-Shrauner*, 1972]. For each of the described methods, we determine the shock orientation, shock speed, and asymptotic upstream and downstream plasma values and their uncertainties in the rest frame of the shock. The plasma values are then used to calculate sound, Alfvén, and magnetosonic wave speeds, and, combined with angles the shock makes with the upstream and downstream fields, the slow, intermediate, and fast wave speeds. These speeds and angles are then used to derive any desired fast, slow or critical Mach numbers. For each derived parameter we store the uncertainty in the derivation based on each method, and the overall standard deviation in the value between all of the analysis methods.

[22] We have employed this large number of shock analysis methods because we find that often many of the methods produce a very similar result, while one or two techniques (often the velocity or magnetic coplanarity methods) produce very different results. For each shock the results from each method are compared, outliers are rejected, and a consensus orientation is determined. As has been noted previously [*Szabo*, 1994], it can sometimes be difficult to identify an asymptotic interval, especially in the disturbed region downstream of a shock where fluctuations and sometimes coherent oscillations may be observed. Sometimes, however, even in the presence of these fluctuations, the different methods all produce similar results, and the event is kept in the list of analyzed shocks. If none of the methods agree, or if there is a large uncertainty in the derived parameters, then the shock is marked as questionable and not used in further analysis. Finally, some of the events turn out to be simple discontinuities and not shocks. They are tracked in the database but also excluded.

[23] While the database includes fast, slow, forward, and reverse IP shocks, only fast mode forward shocks were analyzed in this study. In addition to the reasons described above, shocks were also eliminated from this study for other factors, including proximity to the terrestrial foreshock region, concurrent radio signals such as Type III radio bursts, and gaps in the TNR instrument data set. After this selection process, 178 shocks suitable for analysis remained.

[24] Each selected shock was analyzed for large increases in power at the plasma frequency line in the upstream region. In the TNR data, the plasma line is an ubiquitous feature, located roughly at the plasma frequency, created by the potential fluctuations which arise on the antenna due to electron thermal motion [*Meyer-Vernet and Perche*, 1989]. Langmuir waves also appear at the plasma frequency, as a bursty feature with a much higher intensity than the plasma line from the thermal noise. In order to automatically determine which IP shocks exhibit Langmuir waves, the detection algorithm compares the peak upstream power in the vicinity of the plasma line with the background power from the thermal noise spectrum.

[25] The following simple algorithm was used to fit the plasma line upstream of each shock. First, the plasma density, as measured by the PESA-L instrument from the Wind 3DP plasma suite [*Lin et al.*, 1995], was used as an estimate of the plasma frequency. A detection algorithm found the plasma peak by searching for the highest TNR value in the vicinity of the expected plasma frequency. The total power in the plasma line for each TNR sample was estimated by summing several bins around the peak bin.

[26] Each shock is assigned a designated score (P_{LW}/P_{f_p}) determined by the ratio of the maximum "Langmuir wave" power to the "plasma wave" power, i.e., the maximum power occurring in a short and bursty interval versus a baseline of quiet time power. The P_{LW}/P_{f_p} scores for the shocks in the database range from 1.03, for a very quiet and steady upstream region, to 115.16, for a shock with the largest measured upstream Langmuir waves. We choose a P_{LW}/P_{f_p} score of 10 as the threshold to separate the shocks into two populations, those with upstream LWA and those without. Section 5 describes the selection of this threshold in further detail.

[27] Figure 2 shows several examples of the Langmuir wave detection algorithm, using three example shocks. The first panel in each plot shows the GSE magnetic field $\mathbf{B}_{GSE}$ from MFI. The second panel shows the proton density n_p as measured by PESA-L. The arrival of the shock can be seen as a sharp jump in plasma density and a discontinuity in the magnetic field. The red vertical line on each plot shows the time of shock arrival, and the black vertical lines delimit the upstream interval where the algorithm searches for Langmuir waves. The third panel shows the spectrogram from TNR. The black and white dashed lines superimposed on the TNR spectrogram show the frequency window containing the bins summed to yield the plasma line power. The

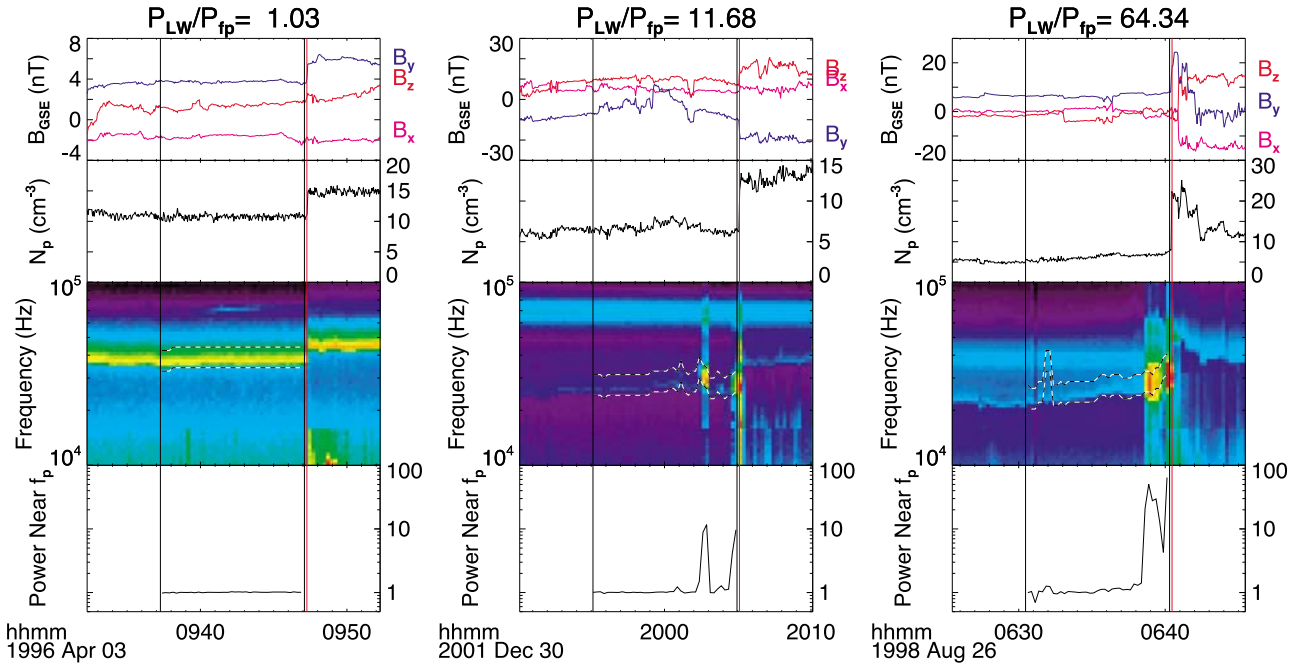

Figure 2. Three example shocks illustrating the Langmuir wave detection algorithm described in section 3. Shown are the GSE magnetic field (first panel), the proton density (second panel), a spectrogram from the WAVES/TNR instrument (third panel), and the power in the vicinity of the plasma line measured by TNR (fourth panel). Large, bursty increases in the power near the plasma line indicate Langmuir waves. The red vertical line marks the arrival of the shock, and the upstream region is denoted by black vertical lines. The white and black dashed lines on the spectrogram show the window over which the TNR power was summed to yield the plasma line power.

fourth panel shows the power close to the plasma frequency in the upstream region.

[28] Figure 2 (left) is an example of a shock with a quiet, steady upstream region. There is almost no variation in the upstream plasma frequency power, and the shock is assigned a low P_{LW}/P_{f_p} score of 1.03. Figure 2 (middle) shows a shock with moderate levels of LWA (P_{LW}/P_{f_p} = 11.68), as shown by two short bursts of increased power near the plasma line. Figure 2 (right) shows a shock with very strong upstream LWA (P_{LW}/P_{f_p} = 64.34.) This shock has been previously studied [*Bale et al.*, 1999; *Pulupa and Bale*, 2008], using in situ wave and particle measurements.

4. KS Test and Parameter Testing

4.1. Test Procedure

[29] As shown in sections 1–3, the basic mechanism for acceleration of electrons at IP shocks is reasonably well understood, i.e., the electrons are reflected from quasi-perpendicular connection sites via a fast Fermi process. In this respect, IP foreshocks are directly analogous to the terrestrial electron foreshock. However, while the terrestrial foreshock is a steady state feature of the interaction between the terrestrial magnetosphere and the solar wind, foreshock regions are only seen at a minority of IP shock crossings. Because foreshock regions occupy only a limited area of any given shock front, there is no way to predict with certainty whether an individual IP shock will show evidence of an IP foreshock region for a single spacecraft encounter. We therefore must use statistical methods to determine the effect of individual shock or plasma parameters on the production of upstream electrons and the resultant Langmuir waves.

[30] The statistical procedure we use for a given parameter x is as follows: choose a threshold value of the P_{LW}/P_{f_p} score described in section 3, and from that threshold determine which shocks exhibit upstream LWA. Next, compare the distribution of parameter x for all observed shocks to the distribution of x for the shocks with LWA. We use the Kolmogorov-Smirnov (KS) test to compare the two distributions [*Press et al.*, 1992, section 14]. The KS test for two sample distributions works by comparing the cumulative distribution functions (CDFs) $S_{N1}(x)$ and $S_{N2}(x)$ of the two samples. The KS statistic D_{KS} measures the maximum distance between the two CDFs:

$$D_{KS} = \max_{-\infty<x<\infty} |S_{N1}(x) - S_{N2}(x)| \quad (3)$$

[31] The D_{KS} statistic is a measure of the difference between two distributions. Two samples drawn from the same distribution will lay atop each other when the CDF is plotted (see the M_f plot in Figure 3 for an example) and will therefore have a small D_{KS}, while samples from different distributions will show significant differences (see the V_{HT} plot in Figure 3) and D_{KS} will be large. Given the number of samples and the D_{KS} statistic, the probability (P_{KS}) that the samples are from the same underlying distribution can be

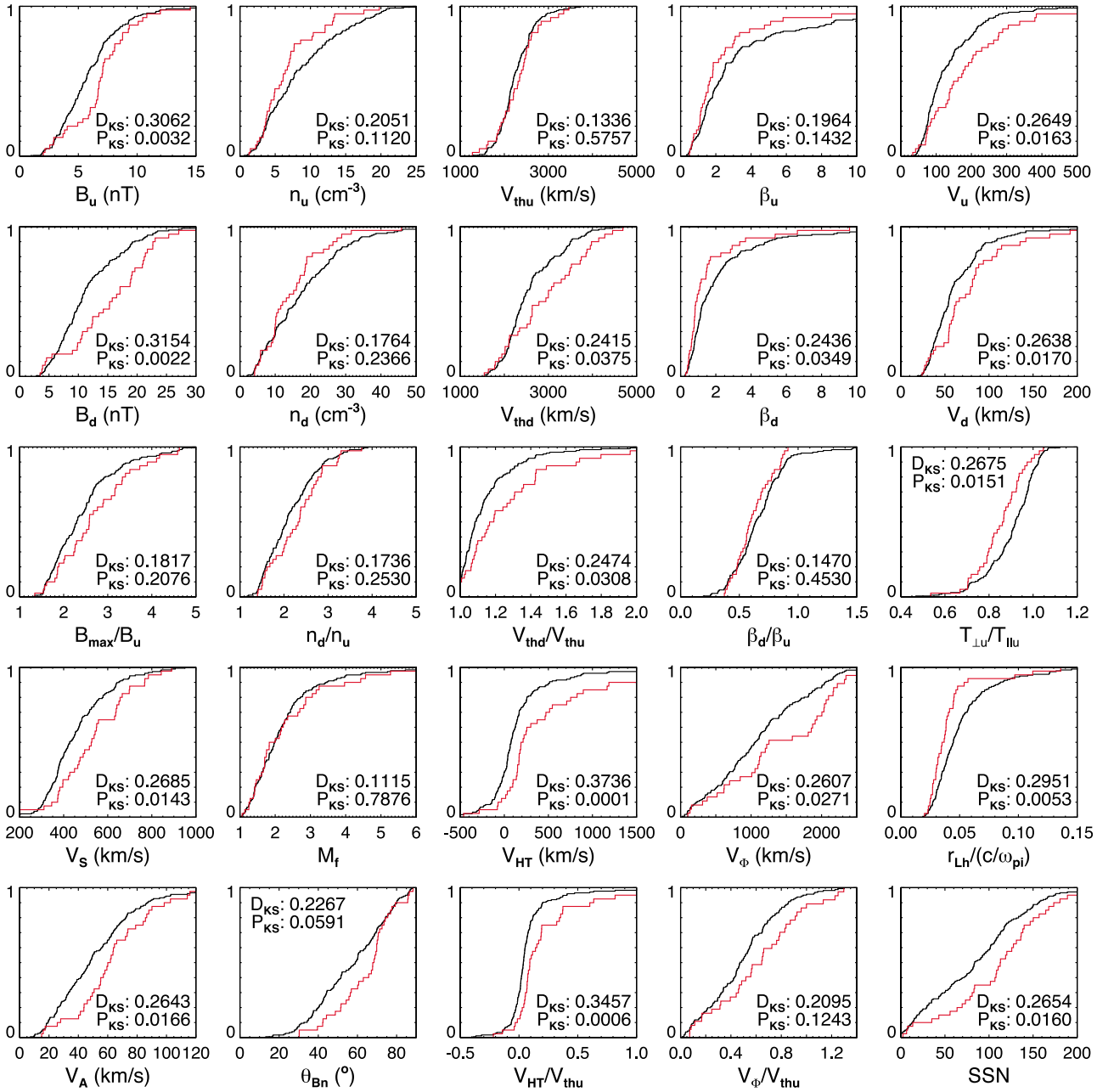

Figure 3. Results of the Kolmogorov-Smirnov test for the selected shock and plasma parameters. The black line shows the CDF for all shocks. The red line shows the CDF for the subset of shocks which exhibit upstream Langmuir waves. The maximum difference between the two populations (the D_{KS} statistic) can be used to calculate the probability (P_{KS}) that the two populations come from the same underlying distribution.

calculated. Parameters with greater influence on the generation of upstream Langmuir waves will have larger differences between the two distributions and, therefore, smaller values of P_{KS}.

4.2. Tested Parameters

[32] The above procedure can be applied to any continuous shock or plasma parameter and used to determine whether it is correlated with upstream LWA. In this section we list the selected test parameters and explain their relevance to electron acceleration or the formation of foreshock regions. All of the tested parameters, along with the results of the tests, are shown in Figure 3.

[33] We test the upstream and downstream magnetic field B_u and B_d, as well as the magnetic compression ratio B_{max}/B_u. When calculating the mirror ratio, we use B_{max}, the maximum value of the magnetic field through the shock transition, including the overshoot region if it is present,

since the electron mirror ratio is determined by the maximum B encountered during the reflection process. The downstream magnetic field is measured after any overshoot or undershoot structure. We also test the analogous densities, n_u, n_d, and n_d/n_u, although we use the asymptotic downstream value to calculate the density compression.

[34] As can be seen from Figure 1, hot electron distribution will contain more electrons which lie above the loss cone in velocity space and can be reflected. The measurement of the downstream thermal velocity V_{thd} is a measurement of electron heating by the shock, as discussed by *Fitzenreiter et al.* [2003]. We test both the upstream and downstream thermal speeds as well as the ratio V_{thd}/V_{thu}. Although the majority of reflected electrons come from the halo portion of the solar wind distribution function, we use the core electron temperature to determine V_{th}. This choice was made for ease of computation, and is justified by the correlation between the core and halo temperatures [*Feldman et al.*, 1975]. The reflection process will also be affected by temperature anisotropies in the solar wind electron distribution, for this reason we calculate and test the ratio between the perpendicular and parallel electron temperatures, $T_\perp/T_\parallel$.

[35] Plasma β, the ratio of plasma pressure to magnetic pressure, has been linked to the nonstationary structure of shocks [see, e.g., *Hellinger et al.* 2002]. We use the total plasma β, including contributions from both ions and electrons. We test β_u and β_d, as well as the ratio β_d/β_u. We also measure and test the upstream and downstream solar wind velocities in the shock frame, V_u and V_d.

[36] In addition to the above solar wind plasma parameters, we test various derived shock parameters. M_f, the fast mode Mach number, given by $M_f = V_u/V_f$, where V_f is the speed of the fast mode wave, is a measure of the strength of the shock. The transition from subcritical to supercritical Mach number is generally associated with changes in upstream shock structure due to reformation, and occurs at a fast wave Mach number of 1–2 for typical solar wind plasma conditions [*Edmiston and Kennel*, 1984]. *Thejappa and MacDowall* [2000] found that shocks with Langmuir waves tend to be supercritical.

[37] V_s is the measured shock speed in the spacecraft frame, calculated as described in section 3. For CME-driven shocks, higher CME and shock speeds are associated with increased probability that a given CME will drive a Type II-producing shock [*Cane et al.*, 1987; *Gopalswamy et al.*, 2005].

[38] Figure 1 shows the effect of V_{HT} and Φ' on the electron reflection process, so these variables are a natural choice to test. Since the fraction of electrons which lie above the velocity space separatrix is dependent on the thermal speed of the electrons, we also test the two parameters normalized to the upstream electron thermal velocity.

[39] V_{HT} is calculated according to equation (1). V_Φ is obtained by setting $v'_\perp = 0$ in equation (2) and solving for $v'_\perp$. If we approximate Φ' using the relation $e\Delta\Phi' \approx 2\Delta T_e$ [*Hull et al.*, 2000], then

$$V_\Phi/V_{th} = \left(2\frac{T_d - T_u}{T_u}\frac{B_u}{B_d - B_u}\right)^{1/2} \tag{4}$$

[40] Figure 1 shows that a V_Φ/V_{th} ratio close to or above 1 implies that most of the core electrons cannot be reflected by the shock. This condition obtains for most IP shocks in this study, implying that the halo population is especially important for the formation of the electron beam.

[41] The fast Fermi theory relies on the adiabatic nature of the electron encounter with the shock. We test $r_{Lh}/(c/\omega_{pi})$, the electron Larmor radius divided by the ion inertial length, to check the validity of this assumption. Simulations [e.g., *Burgess*, 2006] show that substructure exists within shock transition regions which is on the order of the ion inertial length c/ω_{pi}, so this is the relevant length scale for reflection. Therefore, the ratio of a halo electron Larmor radius to c/ω_{pi} is a measure of how well the assumption of small gyroradius (and therefore adiabatic motion) ought to hold. Numerically, $r_{Lh}/(c/\omega_{pi})$ is equivalent to $(mv_h)/(Mv_A)$ and is given by:

$$\frac{r_{Lh}}{c/\omega_{pi}} = \left(\frac{mv_h}{eB}\right)\frac{1}{c}\left(\frac{ne^2}{\varepsilon_0 M}\right)^{1/2} = \frac{mv_h}{Mv_A} \approx 0.015\cdot\frac{E_h(\mathrm{eV})^{1/2}\cdot n(\mathrm{cm}^{-3})^{1/2}}{B(\mathrm{nT})} \tag{5}$$

where $E_h = \frac{1}{2}mv_h^2$ is the energy of a halo electron, typically about 6 times the energy of a core electron [*Feldman et al.*, 1975]. We use B_{max}, the maximum magnetic field observed in the shock transition, in equation (5), and the downstream value for the density n_d.

[42] Finally, we calculate and test the effect of SSN, the daily sunspot number, a standard measure of solar activity. The sunspot number used for any given shock is the daily number for the day the shock was launched, as opposed to the day the spacecraft encountered the shock. We choose this convected sunspot number as a rough measure of the complexity of structure in the solar wind through which the shock will propagate.

5. Results

[43] As mentioned in section 3, we choose a threshold value of P_{LW}/P_{f_p} to distinguish between shocks with LWA and those without. In Figure 4 (top), the number of shocks with P_{LW}/P_{f_p} greater than a given threshold (i.e., the number of shocks N_{LW} with LWA) is plotted versus threshold value. A histogram of P_{LW}/P_{f_p} is also plotted. It is not immediately apparent from the N_{LW} plot or the histogram that there are two distinct populations of shocks, although the histogram data shows a minimum around a P_{LW}/P_{f_p} value of 10, possibly indicating a break between populations. To confirm that this value is a good separator, we use the KS test. Figure 4 (bottom) shows variation of P_{KS} with different choices of P_{LW}/P_{f_p} threshold for several of the parameters described in section 4. All parameters start at a P_{KS} value of 1, a result of the trivial equality of the two populations when there is no required increase in activity near the plasma line for a shock to be counted as a Langmuir wave shock. Parameters which have a strong controlling effect on LWA will tend toward low values of P_{KS}. Several of the predictive parameters plotted in Figure 4 (V_{HT}, SSN, B_{max}/B_u) show a sharp downward trend followed by more stable behavior starting at threshold values of ~8–10, justifying use of 10 as a P_{LW}/P_{f_p} threshold. Beyond this point, no parameter shows

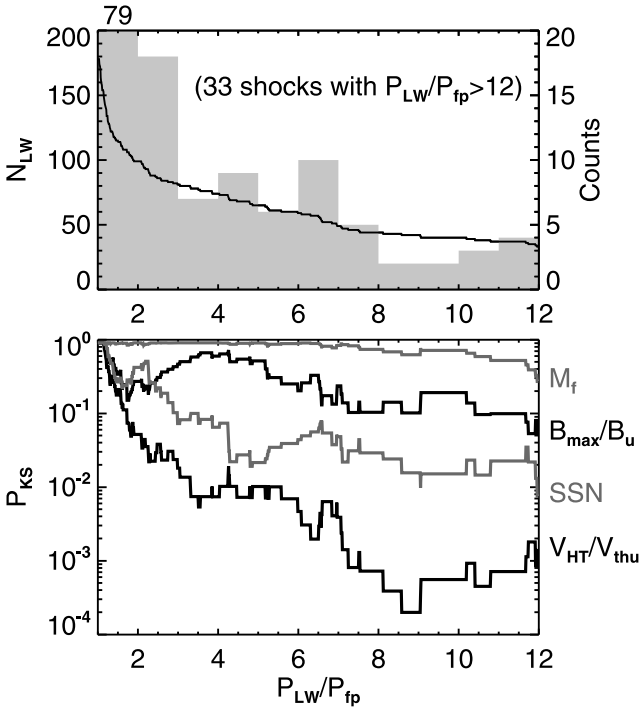

Figure 4. (top) The number of shocks exhibiting upstream Langmuir waves versus threshold P_{LW}/P_{f_p}, showing that there is no clear cutoff value for LWA. A histogram of P_{LW}/P_{f_p} values is also plotted, with the right axis showing the counts in each histogram bin. Seventy-nine shocks lie in the lowest bin. (bottom) P_{KS} values for different threshold values of P_{LW}/P_{f_p}. The P_{KS} statistic varies considerably for many tested parameters for threshold values of P_{LW}/P_{f_p} ranging from 1 to 8, but after 8 the P_{KS} remains fairly steady, justifying the selection of a threshold value of 10.

increased predictive ability. We therefore use for the remainder of this paper a P_{LW}/P_{f_p} score of 10 to separate the two populations of shocks. A total of 43 shocks out of the 178 forward shocks analyzed (24%) produced upstream Langmuir waves, which agrees quite well with the result of *Thejappa and MacDowall* [2000], who observed upstream activity at 31 of 160 interplanetary shocks (19%), and at 22 of 97 forward shocks (23%).

[44] Most tested parameters, both measured and derived, show some association with upstream Langmuir wave activity, as can be seen by examining the CDF plots in Figure 3. The direction of the effect, i.e., whether an increase or decrease in the parameter is associated with activity, is apparent from which direction the red line (shocks with LWA) in the KS plot is shifted compared to the black line (all shocks). The magnitude of the effect is shown by P_{KS}, which is the probability that the LWA CDF for a given parameter could be drawn randomly from the distribution of all shocks. Following *Press et al.* [1992, section 14], we use $P_{KS} \sim 0.2$ as a rough dividing line between parameters which have a significant effect on LWA and those that do not; for parameters with $P_{KS} >\sim 0.2$ the KS test essentially states that there is no statistically significant difference between the two distributions.

[45] Since many of the derived parameters are combinations of the measured parameters, comparing the relative P_{KS} values allows us to determine which components of derived quantities are most crucial to the physics of electron acceleration. For example, the best predictor of LWA is the de Hoffmann-Teller speed V_{HT}. The calculation of V_{HT} incorporates both θ_{bn} and V_u, and comparison of the relative P_{KS} scores shows that V_{HT} is a much better predictor than either measured parameter by itself.

[46] This case can be contrasted with $r_{Lh}/(c/\omega_{pi})$, which is also strongly associated with LWA. However, the absolute strength of the magnetic field are better predictors than the derived quantity $r_{Lh}/(c/\omega_{pi})$, so we can conclude that B is the most important factor in determining the validity of the adiabatic reflection assumption, for the typical range of parameters encountered in the solar wind. In terms of the physics of electron reflection, this corresponds to the fact that in regions of low magnetic field, electrons can become demagnetized and drift away from regions where acceleration is favored.

[47] The strength of the cross shock potential, expressed as a critical velocity V_ϕ for reflection, is also associated with increased LWA. The normalized quantities V_{HT}/V_{th} and V_ϕ/V_{th} are roughly equally good as predictors as the unnormalized quantities, despite the fact that higher thermal velocities should lead to more and higher-energy electrons reflected from the shock front. This contradiction can be explained by observing that V_ϕ is of the order of V_{th}, and that therefore most of the core thermal population of electrons will be drawn through the shock front by the cross shock potential into the downstream region. Therefore, the relevant population of electrons is the halo. Although the density and temperature of the halo are well correlated to the density and temperature of the core [*Feldman et al.*, 1975], the variation in these parameters and the fact that the bulk velocity of the halo may not coincide with the core bulk velocity means that the core thermal speed is an imprecise proxy for the thermal speed of the reflected electrons.

[48] Surprisingly, the temperature anisotropy analysis shows that shocks with low $T_\perp$ are correlated with LWA, despite the fact that high $T_\perp$ should lead to more reflected electrons, according to equation (2). This result may also be due to the difference between the core and halo population; the measured temperature anisotropy we use is for the core population, and the statistics of the halo anisotropy are quite different [*Štverák et al.*, 2008].

[49] A significant finding of *Thejappa and MacDowall* [2000] was that Langmuir waves occur upstream of both quasiperpendicular shocks and quasiparallel shocks. We confirm this finding, however, we find that quasiperpendicular shocks are highly favored to produce upstream waves, as expected from fast Fermi theory. The few instances of quasiparallel shocks with observed LWA may be a result of the fact that the single spacecraft measurement of θ_{bn} is made at the point that the spacecraft crosses the shock, and not at the point on the shock where the electrons are accelerated. Nonplanar shock structure and curvature or diffusion of the upstream magnetic field could cause the measurement of θ_{bn} to differ between these two points.

[50] Both the magnetic compression and the density compression ratios exhibit only a weak relationship with LWA compared to those due to the upstream and down-

Table 1. For Each Tested Parameter, the Kolmogorov-Smirnov Statistic D_{KS} and the Associated Significance P_{KS}, Comparing the Distribution of All Shocks to Shocks With Langmuir Waves, and Using a P_{LW}/P_{fp} Threshold of 10

Quantity	D_{KS}	P_{KS}
V_{HT}	0.3736	0.0001
V_{HT}/V_{thu}	0.3457	0.0006
B_d	0.3154	0.0022
B_u	0.3062	0.0032
$r_{Lh}/(c/\omega_{pi})$	0.2951	0.0053
V_S	0.2685	0.0143
$T_{\perp u}/T_{\parallel u}$	0.2675	0.0151
SSN	0.2654	0.0160
V_u	0.2649	0.0163
V_A	0.2643	0.0166
V_d	0.2638	0.0170
V_Φ	0.2607	0.0271
V_{thd}/V_{thu}	0.2474	0.0308
β_d	0.2436	0.0349
V_{thd}	0.2415	0.0375
θ_{Bn}	0.2267	0.0591
n_u	0.2051	0.1120
V_Φ/V_{thu}	0.2095	0.1243
β_u	0.1964	0.1432
B_{max}/B_u	0.1817	0.2076
n_d	0.1764	0.2366
n_d/n_u	0.1736	0.2530
β_d/β_u	0.1470	0.4530
V_{thu}	0.1336	0.5757
M_f	0.1115	0.7876

stream absolute values of B and n. In the case of the magnetic compression, this implies that the opening angle α of the magnetic mirror has a much smaller influence on the appearance of upstream waves than does B or V_{HT}.

[51] We find that the fast Mach number M_f of the shock is unimportant in predicting LWA. This is true despite the fact that both the shock velocity V_s and the Alfvén velocity V_A are reasonably good predictors of upstream activity. The dependence of LWA on V_A is likely due to the dependence of V_A on B. Since high V_s and high V_A are both correlated with upstream activity and both correlations are comparable in magnitude, the combined effects effectively cancel out dependence on M_f. However, this result is not inconsistent with the findings of *Thejappa and MacDowall* [2000] that most LWA is found upstream of supercritical shocks; we suggest that it is simply a corollary of the fact that most IP shocks are supercritical at helioradial distances equal to or greater than 1 AU.

[52] We also find that the sunspot number is quite good as a predictor of upstream LWA at a given shock. There are two possible explanations for this effect. The first is that the variation in the solar cycle causes variation in shock and plasma parameters which control LWA. Several solar wind parameters are correlated well with solar activity, including wind speed and magnetic field [see, e.g., *Veselovsky et al.*, 2000]. However, electron heat flux does not vary with solar activity [*Scime et al.*, 2001]. The other explanation is that shock structure may be sensitive to the environment into which the shock propagates through the heliosphere. A shock propagating into a relatively quiet solar wind environment, such as that found during periods of low solar activity, encounters a more homogeneous environment than a shock propagating into the relatively variable solar wind existing during periods of intense solar activity. Inhomogeneities may lead to differences in shock formation and a greater level of structure on the front of the shock, creating favorable conditions for the generation of foreshock bays.

[53] Table 1 lists all of the analyzed shock and plasma parameters, in order of decreasing correlation with upstream Langmuir wave activity.

6. Discussion and Summary

[54] The results of section 5 emphasize the complexity of Type II radio burst generation. *Pulupa and Bale* [2008] have shown that the characteristic scale of foreshock bays is on the order of tens to hundreds of Mm, but parameters on scales both significantly smaller ($r_{Lh}/(c/\omega_{pi})$, which describes structure on the scale of the shock width) and significantly larger (SSN, which serves as a proxy of structure in the entire solar wind) than this also play a role in determining the existence of upstream Langmuir waves.

[55] A picture of the dependence of Type II radio bursts on shock and plasma parameters emerges from these results, as follows: An IP shock is launched into the heliosphere. If the shock propagates into a highly inhomogeneous environment, it is likely to develop structure on the shock front, which by 1 AU has the characteristic dimensions of the observed foreshock bays. A shock which forms a foreshock region can accelerate electrons effectively to form electron beams and Langmuir waves, if the following conditions apply: the local HT speed is large compared to the speed of the typical halo electron, and the magnetic field is strong enough to keep the electron bound to a quasiperpendicular acceleration site throughout its encounter with the shock. For a given shock crossing, whether the spacecraft encounters LWA depends on the exact location of the crossing on the shock front.

[56] In summary, we have surveyed a large number of shocks observed by the Wind spacecraft, searching for upstream Langmuir waves using the TNR instrument on Wind/WAVES and statistically analyzing the data set to determine which parameters affect upstream activity. We show that V_{HT} is clearly the best predictor of upstream LWA. This agrees well with the predictions of fast Fermi theory. We confirm the conclusions of *Thejappa and MacDowall* [2000] that LWA occurs upstream of slightly more than 20% of interplanetary fast shocks, and that activity occurs upstream of both quasiperpendicular and quasiparallel shocks. However, we note that there is a strong preference for quasiperpendicular shocks, and that observations of quasiparallel shocks may be an artifact of nonlocal measurements of the upstream connection site. Of the parameters measured by both this study and calculated by *Knock et al.* [2003], we agree that upstream activity is very sensitive to the upstream speed of the shock. However, we find that shocks with lower rather than higher upstream densities are favored for LWA. We show an intriguing relationship between LWA and solar activity, which may indicate that structure in the solar wind leads to corresponding structure on shock fronts. The ratio between the Larmor radius and the ion inertial length is also a good predictor of upstream activity, which suggests that the microphysics of shock

structure also is important. The large number of parameters which are associated with upstream LWA underscores the complexity of Type II burst generation and suggests that a complete model of Type II generation must include both the microphysics of shock structure and the global view of the solar wind into which the IP shock is propagating.

[57] **Acknowledgments.** Work at UC Berkeley is sponsored by the NASA grant NNX08AE34G. Wind/MFI data are courtesy of the MFI team (PI: R. P. Lepping) at Goddard Space Flight Center.

[58] Amitava Bhattacharjee thanks André Mangeney and Robert MacDowall for their assistance in evaluating this paper.

References

Abraham-Shrauner, B. (1972), Determination of magnetohydrodynamic shock normals, *J. Geophys. Res.*, *77*, 736–739, doi:10.1029/JA077i004p00736.

Anderson, K. A. (1968), Energetic electrons of terrestrial origin upstream in the solar wind, *J. Geophys. Res.*, *73*, 2387–2397, doi:10.1029/JA073i007p02387.

Anderson, K. A., R. P. Lin, F. Martel, C. S. Lin, G. K. Parks, and H. Reme (1979), Thin sheets of energetic electrons upstream from the Earth's bow shock, *Geophys. Res. Lett.*, *6*, 401–404, doi:10.1029/GL006i005p00401.

Bale, S. D., M. J. Reiner, J.-L. Bougeret, M. L. Kaiser, S. Krucker, D. E. Larson, and R. P. Lin (1999), The source region of an interplanetary type II radio burst, *Geophys. Res. Lett.*, *26*, 1573–1576, doi:10.1029/1999GL900293.

Bougeret, J.-L., et al. (1995), Waves: The Radio and Plasma Wave Investigation on the Wind spacecraft, *Space Sci. Rev.*, *71*, 231–263, doi:10.1007/BF00751331.

Burgess, D. (2006), Simulations of electron acceleration at collisionless shocks: The effects of surface fluctuations, *Astrophys. J.*, *653*, 316–324, doi:10.1086/508805.

Cairns, I. H., P. A. Robinson, and G. P. Zank (2000), Progress on coronal, interplanetary, foreshock, and outer heliospheric radio emissions, *Publ. Astron. Soc. Aust.*, *17*, 22–34.

Cane, H. V., R. G. Stone, J. Fainberg, J. L. Steinberg, S. Hoang, and R. T. Stewart (1981), Radio evidence for shock acceleration of electrons in the solar corona, *Geophys. Res. Lett.*, *8*, 1285–1288, doi:10.1029/GL008i012p01285.

Cane, H. V., R. G. Stone, J. Fainberg, J. L. Steinberg, and S. Hoang (1982), Type II solar radio events observed in the interplanetary medium. I - General characteristics, *Sol. Phys.*, *78*, 187–198, doi:10.1007/BF00151153.

Cane, H. V., N. R. Sheeley Jr., and R. A. Howard (1987), Energetic interplanetary shocks, radio emission, and coronal mass ejections, *J. Geophys. Res.*, *92*, 9869–9874, doi:10.1029/JA092iA09p09869.

Cremades, H., O. C. St. Cyr, and M. L. Kaiser (2007), A tool to improve space weather forecasts: Kilometric radio emissions from Wind/WAVES, *Space Weather*, *5*, S08001, doi:10.1029/2007SW000314.

Edmiston, J. P., and C. F. Kennel (1984), A parametric survey of the first critical Mach number for a fast MHD shock, *J. Plasma Phys.*, *32*, 429–441.

Feldman, W. C., J. R. Asbridge, S. J. Bame, M. D. Montgomery, and S. P. Gary (1975), Solar wind electrons, *J. Geophys. Res.*, *80*, 4181–4196, doi:10.1029/JA080i031p04181.

Feldman, W. C., R. C. Anderson, S. J. Bame, S. P. Gary, J. T. Gosling, D. J. McComas, M. F. Thomsen, G. Paschmann, and M. M. Hoppe (1983), Electron velocity distributions near the Earth's bow shock, *J. Geophys. Res.*, *88*, 96–110, doi:10.1029/JA088iA01p00096.

Filbert, P. C., and P. J. Kellogg (1979), Electrostatic noise at the plasma frequency beyond the Earth's bow shock, *J. Geophys. Res.*, *84*, 1369–1381, doi:10.1029/JA084iA04p01369.

Fitzenreiter, R. J., K. W. Ogilvie, S. D. Bale, and A. F. Viñas (2003), Modification of the solar wind electron velocity distribution at interplanetary shocks, *J. Geophys. Res.*, *108*(A12), 1415, doi:10.1029/2003JA009865.

Goodrich, C. C., and J. D. Scudder (1984), The adiabatic energy change of plasma electrons and the frame dependence of the cross-shock potential at collisionless magnetosonic shock waves, *J. Geophys. Res.*, *89*, 6654–6662, doi:10.1029/JA089iA08p06654.

Gopalswamy, N., E. Aguilar-Rodriguez, S. Yashiro, S. Nunes, M. L. Kaiser, and R. A. Howard (2005), Type II radio bursts and energetic solar eruptions, *J. Geophys. Res.*, *110*, A12S07, doi:10.1029/2005JA011158.

Gurnett, D. A., F. M. Neubauer, and R. Schwenn (1979), Plasma wave turbulence associated with an interplanetary shock, *J. Geophys. Res.*, *84*, 541–552, doi:10.1029/JA084iA02p00541.

Hellinger, P., P. Trávníček, and H. Matsumoto (2002), Reformation of perpendicular shocks: Hybrid simulations, *Geophys. Res. Lett.*, *29*(24), 2234, doi:10.1029/2002GL015915.

Hoang, S., M. Maksimovic, J.-L. Bougeret, M. J. Reiner, and M. L. Kaiser (1998), Wind-Ulysses source location of radio emissions associated with the January 1997 coronal mass ejection, *Geophys. Res. Lett.*, *25*, 2497–2500, doi:10.1029/98GL00571.

Hull, A. J., J. D. Scudder, R. J. Fitzenreiter, K. W. Ogilvie, J. A. Newbury, and C. T. Russell (2000), Electron temperature and de Hoffmann-Teller potential change across the Earth's bow shock: New results from ISEE 1, *J. Geophys. Res.*, *105*, 20,957–20,972, doi:10.1029/2000JA900049.

Kasper, J. C., A. J. Lazarus, J. T. Steinberg, K. W. Ogilvie, and A. Szabo (2006), Physics-based tests to identify the accuracy of solar wind ion measurements: A case study with the Wind Faraday Cups, *J. Geophys. Res.*, *111*, A03105, doi:10.1029/2005JA011442.

Knock, S. A., I. H. Cairns, P. A. Robinson, and Z. Kuncic (2001), Theory of type II radio emission from the foreshock of an interplanetary shock, *J. Geophys. Res.*, *106*, 25,041–25,052, doi:10.1029/2001JA000053.

Knock, S. A., I. H. Cairns, P. A. Robinson, and Z. Kuncic (2003), Theoretically predicted properties of type II radio emission from an interplanetary foreshock, *J. Geophys. Res.*, *108*(A3), 1126, doi:10.1029/2002JA009508.

Krauss-Varban, D., and D. Burgess (1991), Electron acceleration at nearly perpendicular collisionless shocks: 2. Reflection at curved shocks, *J. Geophys. Res.*, *96*, 143–154, doi:10.1029/90JA01728.

Krauss-Varban, D., D. Burgess, and C. S. Wu (1989), Electron acceleration at nearly perpendicular collisionless shocks: 1. One-dimensional simulations without electron scale fluctuations, *J. Geophys. Res.*, *94*, 15,089–15,098, doi:10.1029/JA094iA11p15089.

Larson, D. E., et al. (1996), Probing the Earth's bow shock with upstream electrons, *Geophys. Res. Lett.*, *23*, 2203–2206, doi:10.1029/96GL02382.

Lepping, R. P., et al. (1995), The Wind Magnetic Field Investigation, *Space Sci. Rev.*, *71*, 207–229, doi:10.1007/BF00751330.

Leroy, M. M., and A. Mangeney (1984), A theory of energization of solar wind electrons by the Earth's bow shock, *Ann. Geophys.*, *2*, 449–456.

Lin, R. P., et al. (1995), A three-dimensional plasma and energetic particle investigation for the Wind spacecraft, *Space Sci. Rev.*, *71*, 125–153, doi:10.1007/BF00751328.

Meyer-Vernet, N., and C. Perche (1989), Tool kit for antennae and thermal noise near the plasma frequency, *J. Geophys. Res.*, *94*, 2405–2415, doi:10.1029/JA094iA03p02405.

Ogilvie, K. W., et al. (1995), SWE, a comprehensive plasma instrument for the Wind spacecraft, *Space Sci. Rev.*, *71*, 55–77, doi:10.1007/BF00751326.

Potter, D. W. (1981), Acceleration of electrons by interplanetary shocks, *J. Geophys. Res.*, *86*, 11,111–11,116, doi:10.1029/JA086iA13p11111.

Press, W. H., S. A. Teukolsky, W. T. Vetterling, and B. P. Flannery (1992), *Numerical Recipes in FORTRAN: The Art of Scientific Computing*, 2nd ed., Cambridge University Press, Cambridge, U. K.

Pulupa, M., and S. D. Bale (2008), Structure on interplanetary shock fronts: Type II radio burst source regions, *Astrophys. J.*, *676*, 1330–1337, doi:10.1086/526405.

Reiner, M. J., M. L. Kaiser, J. Fainberg, J.-L. Bougeret, and R. G. Stone (1998), On the origin of radio emissions associated with the January 6–11, 1997, CME, *Geophys. Res. Lett.*, *25*, 2493–2496, doi:10.1029/98GL00138.

Richardson, I. G., et al. (2006), Major geomagnetic storms (Dst < = −100 nT) generated by corotating interaction regions, *J. Geophys. Res.*, *111*, A07S09, doi:10.1029/2005JA011476.

Scarf, F. L., R. W. Fredricks, L. A. Frank, and M. Neugebauer (1971), Nonthermal electrons and high-frequency waves in the upstream solar wind: 1. Observations, *J. Geophys. Res.*, *76*, 5162–5171, doi:10.1029/JA076i022p05162.

Scime, E. E., J. E. Littleton, S. P. Gary, R. Skoug, and N. Lin (2001), Solar cycle variations in the electron heat flux: Ulysses observations, *Geophys. Res. Lett.*, *28*, 2169–2172, doi:10.1029/2001GL012925.

Szabo, A. (1994), An improved solution to the "Rankine-Hugoniot" problem, *J. Geophys. Res.*, *99*, 14,737–14,746, doi:10.1029/94JA00782.

Thejappa, G., and R. J. MacDowall (2000), Langmuir waves in the vicinity of interplanetary shocks and the consequences for Type II burst models, *Astrophys. J.*, *544*, L163–L167, doi:10.1086/317303.

Štverák, Š., P. Trávníček, M. Maksimovic, E. Marsch, A. N. Fazakerley, and E. E. Scime (2008), Electron temperature anisotropy constraints in the solar wind, *J. Geophys. Res.*, *113*, A03103, doi:10.1029/2007JA012733.

Veselovsky, I., A. V. Dmitriev, A. V. Suvorova, and M. V. Tarsina (2000), Solar wind variation with the cycle, *J. Astrophys. Astron.*, *21*, 423–429.

Vinas, A. F., and J. D. Scudder (1986), Fast and optimal solution to the "Rankine-Hugoniot problem," *J. Geophys. Res.*, *91*, 39–58, doi:10.1029/JA091iA01p00039.

Wilson, L. B., III, C. Cattell, P. J. Kellogg, K. Goetz, K. Kersten, L. Hanson, R. MacGregor, and J. C. Kasper (2007), Waves in interplanetary shocks: A Wind/WAVES study, *Phys. Re. Lett.*, *99*(4), 041101, doi:10.1103/PhysRevLett.99.041101.

Wu, C. S. (1984), A fast Fermi process: Energetic electrons accelerated by a nearly perpendicular bow shock, *J. Geophys. Res.*, *89*, 8857–8862, doi:10.1029/JA089iA10p08857.

Zhang, J., et al. (2007), Solar and interplanetary sources of major geomagnetic storms (Dst <= −100 nT) during 1996–2005, *J. Geophys. Res.*, *112*, A10102, doi:10.1029/2007JA012321.

S. D. Bale and M. P. Pulupa, Space Sciences Laboratory, University of California, 7 Gauss Way, Berkeley, CA 94708, USA. (bale@ssl.berkeley.edu; pulupa@ssl.berkeley.edu)

J. C. Kasper, Harvard-Smithsonian Center for Astrophysics, 60 Garden St., Cambridge, MA 02138, USA. (jkasper@cfa.harvard.edu)